JOURNAL OF COMPUTATIONAL PHYSICS 88, 337–361 (1990)

On Applications of a Complex Variable Method in Compressible Flows

PRABIR DARIPA

Division of Applied Mathematics, Department of Mathematics
Texas A & M University, College Station, Texas 77843

Received December 6, 1988; June 26, 1989

In this paper, we develop a complex variable formulation for the potential equations of compressible fluid flow and discuss the possibility of its application to the solution of compressible fluid flow problems. A numerical method to solve inverse problems using this formulation is discussed.

1. INTRODUCTION

In this paper we discuss the complex variable formulation of compressible fluid flow equations and its application to inverse problems. This paper shoud be viewed as an attempt to extend the complex variable approach (CVA) to compressible fluid flow computation. As we know the success of CVA with incompressible flow lies in the Cauchy–Riemann formulation of the fluid flow equations. This suggests that a similar formulation for compressible fluid flow equations may prove useful for many applications. As it turns out, the compressible fluid flow equations admit an almost similar representation in an appropriate plane [1, 2]. The equations in this plane are the nonlinear Cauchy–Riemann equations (CRE). As we will see, the nonlinearity in this plane is very mild in the sense that these equations are linear CRE with an $O(M^4)$ nonlinear contribution, where M is the local Mach number.

This formulation has a number of significant applications and is likely to be useful in fluid flow applications. A similar notion using the partial differential equation in the real plane has been first used by the author [2] and has proven useful in aerodynamic application. Neglecting the nonlinear contribution provides an almost exact solution by a simple fast Fourier transform. The principle idea has been to compute this almost exact solution and then to use this as a driver to get the exact solution. This approach is naturally favorable provided the nonlinear contribution can be computed economically. In [2] the appropriate partial differential equations were solved using this approach and proved quite economical. There a clever approach is taken to remove some of the singularities. Such singularities are encountered at the stagnation points.

As differential operators are not suitable to deal with such singularities, we feel that it is worthwhile to attempt an alternate approach that has inherent

0021-9991/90 $3.00

smoothing properties. It is well known that integral operators provide smoothing of singularities and thus help in dealing with the singularities numerically. In addition, these are also stable with respect to roundoff error. Here we take such an approach by reformulating the compressible fluid flow equations in the complex plane. The integral equation approach we take here allows us to include the $O(M^4)$ correction by computing the nonlinear contribution. However, this might be expensive numerically since multiple integral evaluation is usually involved with such a nonlinear contribution. Even though such is the case with this method at present, the numerical computations of the integral involved can be accelerated by using the ideas of [3, 4]. In any case this is a topic of further research.

The rest of the paper is laid out as follows: In Section 2 we discuss the formulation of the potential equations of compressible fluid flow. In Section 3 we formulate the inverse problem using the theory developed in Section 2. In Section 4 we discuss some special cases. In Section 5 we discuss in some detail the airfoil design problem in the spirit of Section 3. In Section 6 we outline the numerical method and in Section 7 we present some numerical results. Finally, we conclude in Section 8.

2. The Formulation

The potential equations of compressible fluid flow are [1]

$$\nabla \cdot (\rho \vec{q}) = 0; \qquad \nabla \times \vec{q} = 0; \qquad p = \rho^{\gamma}. \tag{1}$$

Here the variables are normalized by their sonic values and linear dimensions by some appropriate linear dimension. Alternately we write (1) as

$$\rho \vec{q} = \nabla \times (c\psi \vec{k}); \qquad \vec{q} = \nabla \phi. \tag{2}$$

The constant c is arbitrary. An appropriate choice of c will play a crucial role in certain estimates and in the numerical method to be discussed later. The above equations in the potential plane are given by [1, 2]

$$\theta_{\phi} - K^{-1} v_{\psi} = 0, \qquad \theta_{\psi} + K v_{\phi} = 0. \tag{3}$$

Above and below ϕ, ψ, θ, v respectively denote the potential, the stream function, the flow direction, and the Prandtl–Meyer function. K and v in (3) are defined as

$$K = c \frac{\beta}{\rho(q(M))}; \qquad v = \int_1^q \frac{\beta \, dq}{q}. \tag{4, 5}$$

We use the notation $\beta^2 = 1 - M^2$. The density ρ is related to the Mach number M and the speed q through Bernoulli's law and the pressure-density relation for an ideal gas. For the γ-law gas, the constant c is chosen to be

$$c = \left(\frac{\gamma + 1}{2} \right)^{1/(\gamma - 1)}. \tag{6}$$

The justification for this particular choice will be made later. With this choice of the constant c, the following relations hold [5]:

$$\frac{c}{\rho}=\left(1+\frac{\gamma-1}{2}M^2\right)^{1/(\gamma-1)}, \tag{7}$$

$$q=\frac{\sqrt{(\gamma+1)/2}\,M}{\sqrt{1+(\gamma-1)/2\,M^2}}, \tag{8}$$

and

$$v=k\tan h^{-1}\left(\frac{\beta}{k}\right)-\tan h^{-1}\beta. \tag{9}$$

In Eq. (9), $k^2=(\gamma+1)/(\gamma-1)$ and we have $0\leqslant K\leqslant 1$ for $1\leqslant M\leqslant 0$. Next we reduce the system (3) to the Beltrami equation in the complex plane.

2.1 *Beltrami Equation*

We introduce the new variables

$$\omega=\phi+i\psi; \qquad \tau=-v+i\theta \tag{10}$$

and define the complex derivatives τ_ω and $\tau_{\bar\omega}$ as formal differential operators given by

$$\tau_{\bar\omega}=\tfrac{1}{2}(\tau_\phi+i\tau_\psi); \qquad \tau_\omega=\tfrac{1}{2}(\tau_\phi-i\tau_\psi). \tag{11}$$

By making use of (3) and (10) in (11), we obtain

$$\tau_{\bar\omega}=\frac{1-K}{2}[K^{-1}\theta_\psi+i\theta_\phi]; \qquad \tau_\omega=\frac{1+K}{2}[K^{-1}\theta_\psi+i\theta_\phi]. \tag{12}$$

It follows from (12) that

$$\tau_{\bar\omega}=\mu\tau_\omega, \tag{13}$$

where μ is given by

$$\mu=\frac{1-K}{1+K}. \tag{14}$$

We denote respectively the domains in z and ω plane by Ω_z and Ω_ω. The mapping $\omega(z)\colon \Omega_z\to\Omega_\omega$ is one-to-one since the Jacobian of this mapping $J=\partial(\phi,\psi)/\partial(x,y)=\rho q^2$ is not zero except at stagnation points.

Equation (13) is known as the Beltrami equation [6]. Equation (13) can be viewed as describing a mapping from the ω plane to the τ plane. Such a mapping exhibits branch-point singularities for many flows in the τ-plane and hence need not be one-to-one [1].

2.2 *Properties of the Coefficient* μ

We mention here the following properties of the coefficient μ given by (14):

(1) Since $\rho(\omega)$ and $\beta(\omega)$ are in $C^\infty(\Omega_\omega)$ (since the flow is subsonic), the functions K and hence μ are also in $C^\infty(\Omega_\omega)$ (see (4) and (14)).

(2) μ is a monotonically increasing function of M, since we obtain from (4) and (14)

$$\frac{dK}{dM} = c\beta \frac{d}{dM}\left(\frac{1}{\rho}\right) + \frac{c}{\rho}\frac{d}{dM}(\beta)$$

$$= -\frac{c\beta}{\rho^2}\frac{d\rho}{dM} - \frac{cM}{\rho\beta} < 0$$

and

$$\frac{d\mu}{dK} = -\frac{2}{(1+K^2)} < 0$$

which gives

$$\frac{d\mu}{dM} = \frac{dM}{dK} * \frac{dK}{d\mu} > 0. \tag{15}$$

(3) μ is positive and bounded between 0 and 1.

Proof. From (4) and (7), we have

$$\mu = \begin{cases} 0, & \text{for } M = 0 \\ 1, & \text{for } M = 1. \end{cases}$$

Then from (15) it follows that

$$0 \leqslant \mu \leqslant 1 \qquad \text{for } 0 \leqslant M \leqslant 1.$$

(4) μ is $O(M^4)$.

Proof. Expanding c/ρ and β in powers of M^2, we have

$$\frac{c}{\rho} = \left(1 + \frac{\gamma - 1}{2} M^2\right)^{1/(\gamma-1)}$$

$$= 1 + \frac{M^2}{2} + \frac{2-\gamma}{8} M^4 + O(M^6) \tag{17}$$

and

$$\beta = (1 - M^2)^{1/2}$$

$$= 1 - \frac{M^2}{2} - \frac{M^4}{8} + O(M^6). \tag{18}$$

From (17) and (18) we have

$$K = \beta \frac{c}{\rho}$$

$$= 1 - \frac{\gamma + 1}{8} M^4 + O(M^6). \tag{19}$$

Hence from (14) and (19) we have

$$\mu = \frac{1-K}{1+K} = \frac{(1-K)/2}{(1-(1-K)/2)}$$

$$= \left(\frac{1-K}{2}\right) + \left(\frac{1-K}{2}\right)^2 + \cdots$$

$$= \frac{\gamma+1}{16} M^4 + \left(\frac{\gamma+1}{16}\right)^2 M^8 + O(M^{12}). \tag{20}$$

Notice from (13) and (20) that τ is analytic to $O(M^4)$. This will have considerable implications in the efficiency of the numerical methods that we discuss in Section 5. It should be mentioned that this, in particular, and subsequent estimates pertain to the specific choice of c we have made in (6). If c were chosen to be one instead of the choice in (6), then the above estimate would be $O(1)$ and the numerical method mentioned later would not be as efficient.

2.3. *Properties of the Beltrami Equation*

Equation (13) has some special properties which we discuss under assumptions: (i) $\tau_\omega \neq 0$ and (ii) μ is a known function of ω. Assumption (i) limits the set of flows and assumption (ii) requires approximating μ in a judicious way so that a good solution is obtained. We state these elementary results (see also [6]) about Eq. (13).

PROPOSITION 1. *If $\tau(\omega)$ is a solution of Eq.* (13), *then any analytic function f or τ is also a solution of the same equation since*

$$f_{\bar{\omega}} = f_\tau \tau_{\bar{\omega}} = f_\tau \mu \tau_\omega = \mu f_\omega.$$

PROPOSITION 2. *If Eq.* (13) *defines a mapping from Ω_ω to Ω_τ in one-to-one continuous way and $\tau_\omega \neq 0$ anywhere in Ω_ω, then any solution u of Eq.* (13) *is analytic in Ω_τ (this is the converse of Proposition* (1)), *since*

$$0 = u_{\bar{\omega}} - \mu u_\omega$$

$$= u_\tau \tau_{\bar{\omega}} + u_{\bar{\tau}} \bar{\tau}_{\bar{\omega}} - \mu(u_\tau \tau_\omega + u_{\bar{\tau}} \bar{\tau}_{\bar{\omega}})$$

$$= u_\tau(\tau_{\bar{\omega}} - u\tau_\omega) + u_{\bar{\tau}}(\bar{\tau}_{\bar{\omega}} - u\bar{\tau}_{\bar{\omega}})$$

$$= u_{\bar{\tau}} \bar{\tau}_{\bar{\omega}} (1 - |\mu|^2)$$

implies $u_{\bar{\tau}} = 0$.

Proposition 1 provides a way to generate infinite families of solutions to (13) by finding *analytic* functions of a known solution to (13). Proposition 2 ensures that the problem of finding a solution ω subject to some condition is equivalent to that of finding an analytic function is a suitable plane subject to certain analogues of these conditions.

The above two propositions, however, do not lead to any simplification to general situations where the assumptions leading to the above two propositions do not apply. Such is the case here since the coefficient μ is a nonlinear function of τ and there exist branch points in τ plane for certain flows [1]. We apply the formulation (13) and the ideas discussed here to solving the inverse problem.

3. Inverse Problem

Consider the inverse problem that is typical of exterior flows past a body: To find the unknown profile L_z, from the following data:

$$q = q(s),\ s \in [0, 1] \qquad \text{and} \qquad \theta(z = \infty) = \theta_\infty. \tag{21}$$

Here s is an arclength parameter. The mapping $z(\omega)$ induced by the potential plane formulation (2), maps infinity in Ω_z to infinity in Ω_ω and the unknown profile, L_z, to

$$\psi = 0; \qquad \phi = \int q(s)\, ds. \tag{22}$$

Equation (22) maps the data $q(s)$ onto a slit, L_ω, and also provides the data $q(\phi)$ and hence $v(\phi)$. We notice from Fig. 1 that L_ω is

$$L_\omega: \begin{cases} \psi = 0^+, & \phi \in [0, \phi_B], \\ \psi = 0^-, & \phi \in [0, \phi_{B'}]. \end{cases}$$

where $(\phi, \psi) = (0, 0)$ corresponds to the front stagnation point and $(\phi_B, 0)$, $(\phi_{B'}, 0)$ respectively correspond to upper and lower sides of the rear stagnation point. The gap $BB' = \Delta\phi$ is the circulation Γ.

The inverse problem now reduces to solving (13) subject to the data,

$$\text{Real}[\tau(\phi, \psi = 0)] = -v(\phi), \qquad \phi \in L_\omega \tag{23a}$$

$$\text{Imag}[\tau(\omega = \infty)] = \theta_\infty. \tag{23b}$$

The solution $\tau(\omega) = -v + i\theta$ is then used in the mapping $z(\omega)$ given by [1, 5].

$$z = \int \frac{e^{i\theta}}{q}\left(d\phi + i\frac{c}{\rho}\, d\psi\right) \tag{24}$$

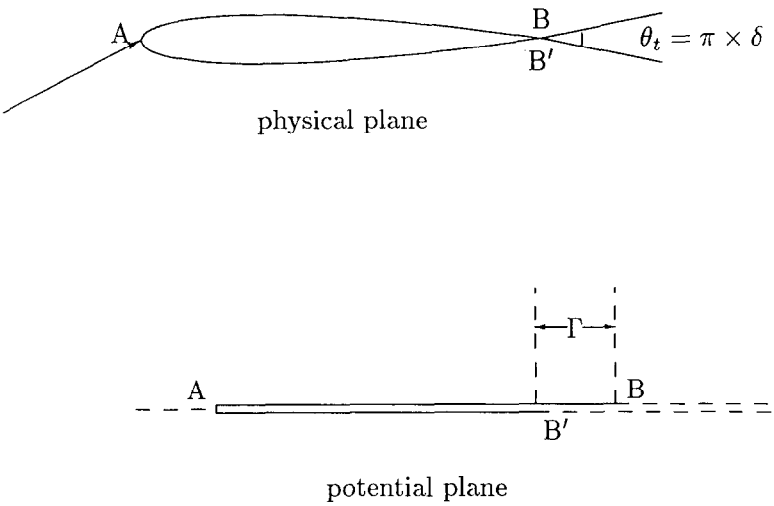

FIG. 1. A typical airfoil in the physical and potential planes.

to construct the flow in Ω_z. In particular, the profile, L_z, is obtained from

$$z = \int \frac{e^{i\theta}}{q}\, d\phi. \tag{25}$$

In order to avoid dealing with the infinite domain in the ω-plane, we define a mapping (conformal)

$$\omega_{\bar{\sigma}} = 0, \tag{26}$$

so that ω plane maps onto the interior of the unit circle $\Omega = \{\sigma : |\sigma| < 1\}$ with a slit $L_\omega \to \partial\Omega(\sigma = e^{i\alpha},\ \alpha \in [0, 2\pi])$. The mapping $\omega(\sigma)\colon \Omega_\omega \to \Omega$ is explicitly given by [2],

$$\omega(\sigma) = a(\sigma e^{i\alpha_0} + \sigma^{-1} e^{-i\alpha_0}) - i2a \sin \alpha_0 \ln(\sigma e^{i\alpha_0}). \tag{27}$$

Here a and α_0 are two constants related to circulation and upstream flow direction. The mapping $\omega(\sigma)$ maps A, A' to $\sigma = 1$ and B to $\sigma = e^{i\alpha_s}$; $\alpha_s = \pi - 2\alpha_0$ (see Fig. 1). From (27), it can be seen that $d\omega/d\sigma \neq 0$ except at these two isolated points on the unit circle and hence this mapping is also one-to-one.

From Eq. (13) and (27), we have in the circle plane,

$$\tau_{\bar{\sigma}} = \chi \tau_\sigma \tag{28}$$

with

$$\chi = \frac{\mu(\overline{\omega_\sigma})}{\omega_\sigma}. \tag{29}$$

An overbar denotes complex conjugate. We note that χ is complex and its magnitude is bounded between 0 and 1, since

$$0 \leqslant |\chi| = \left| \mu \frac{(\overline{\omega_\sigma})}{\omega_\sigma} \right| = |\mu| = \mu \leqslant 1. \tag{30}$$

The right inequality follows from (16). We have used the property that μ is a positive function and is less than one. From (30), it follows that $|\chi|$ has the same properties as those of μ mentioned earlier.

In σ-plane, the boundary data (23a), (23b) maps into

$$\text{Real}(\tau(\sigma = e^{i\alpha})) = -\nu(\alpha); \qquad \alpha \in [0, 2\pi] \tag{31a}$$

$$\text{Imag}(\tau(\sigma = 0)) = \theta_\infty. \tag{31b}$$

The solution of (28) subject to the above boundary data provides us with $\tau(\sigma)$. The profile L_z, which is the image of the unit circle $\sigma = e^{i\alpha}$, is obtained from (see Eq. (25))

$$z(\alpha) = \int_0^\alpha \frac{e^{i\theta}}{q} \frac{d\phi}{d\alpha}\, d\alpha. \tag{32}$$

3.1. *Solution to the Inverse Problem*

We write the solution of (28) as

$$\tau(\sigma) = \tau^p(\sigma) + g(\sigma), \tag{33}$$

where $\tau^p(\sigma)$ is given by (see Appendix A))

$$\tau^p = -\frac{1}{\pi} \iint_{S_\Omega} \frac{\tau_\zeta}{\zeta - \sigma}\, d\xi\, d\eta = -\frac{1}{\pi} \iint_{S_\Omega} \frac{\chi \tau_\zeta}{\zeta - \sigma}\, d\xi\, d\eta. \tag{34}$$

We see that Eq. (33) then satisfies Eq. (28) provided $g(\sigma)$ is an analytic function of σ. Since $\tau(\sigma) - \tau^p(\sigma) = g(\sigma)$ is an analytic function, $g(\sigma)$ is uniquely determined from the boundary values of the real part of $\tau(\sigma) - \tau^p(\sigma)$, except for an arbitrary constant. To fix this arbitrary constant we provide the data (31b). This can be formalized by writing

$$g(\sigma) = h((-\nu(\alpha) - \text{Real}(\tau^p(\alpha)); \theta_\infty), \sigma). \tag{35}$$

where $h(\cdot)$ denotes the functional dependence. For our geometry, $h(\cdot)$ refers to the Poisson's formulae [7]. From (33) and (35) we have

$$\tau(\sigma) = \tau^p(\sigma) + h((-\nu(\alpha) - \text{Real}(\tau^p(\alpha)); \theta_\infty), \sigma). \tag{36}$$

This is a nonlinear integro-differential equation for $\tau(\sigma)$. Therefore the inverse problem is formally solved provided the above equation can be solved for $\tau(\sigma)$.

3.2. *The Algorithm*

We see that Eq. (33), (34), and (35) suggest the following iteration scheme:

$$g_k(\sigma) = h((-v(\alpha) - \text{Real}(\tau_k^p(\alpha)); \theta_\infty), \sigma) \tag{37}$$

$$\tau_k(\sigma) = \tau_k^p(\sigma) + g_k(\sigma) \tag{38}$$

$$\tau_{k+1}^p(\sigma) = T[\tau_k(\zeta); \sigma]. \tag{39}$$

Here the subscript k refers to the level of iteration. T in (39) is the integral operator in (34).

As is obvious, a suitable initial choice of $\tau^p(\sigma)$ starts the iteration procedure. The above scheme updates $\tau^p(\sigma)$ at the end of each iteration and this updated $\tau^p(\sigma)$ becomes the input to the next iteration. The rate of convergence of the above scheme to the exact solution will depend crucially on the initial guess of τ^p. The fact that $\tau^p = O(M^4)$ suggests an initial guess of $\tau^p = 0$. In Section 4 we apply this iteration scheme to a typical inverse problem: the design of an airfoil.

It should be mentioned that regularity of the analytic function $h(\cdot)$ depends on the boundary data $v(\alpha)$ and hence $q(\alpha)$. Since τ is singular when $q = 0$, the extent to which the regularity of Eq. (28) is lost depends directly on the number of zeroes of $q(\alpha)$, $\alpha \in [0, 2\pi]$. This adds to the level of difficulty in solving (28) even numerically using the above iteration scheme.

The data $q(s)$ that is typical of exterior flows of our interest contains at least one zero (flow past a cusped airfoil). The above numerical scheme can easily be adapted to such singular data. We show the details of how to deal with such singular data on a model problem in Section 5.

3.4. *Mapping* $z(\sigma)$: $\Omega \to \Omega_z$

As mentioned earlier, the mapping $\Omega \to \Omega_z$ in one-to-one. The mapping $z(\omega)$: $\Omega_\omega \to \Omega_z$ is given by [1, 2]

$$\begin{aligned} dz &= \frac{e^{i\theta}}{q}\left(d\phi + i\frac{c}{\rho}d\psi\right) \\ &= \frac{e^{i\theta}}{2q}\left\{\left(1+\frac{c}{\rho}\right)d\omega + \left(1-\frac{c}{\rho}\right)d\bar{\omega}\right\} \\ &= \frac{e^{i\theta}}{2q}\left\{\left(1+\frac{c}{\rho}\right)\omega_\sigma d\sigma + \left(1-\frac{c}{\rho}\right)\bar{\omega}_{\bar{\sigma}}d\bar{\sigma}\right\}. \end{aligned} \tag{40}$$

If (ρ, q, θ) are known in the σ-plane, then (40) can be used to map the σ plane to the z-plane. This in essence generates grids in the physical plane. A better understanding of these grids is obtained when we notice from (40),

$$z_\sigma = \frac{e^{i\theta}}{q}\left(1+\frac{c}{\rho}\right)\omega_\sigma; \qquad z_{\bar{\sigma}} = \frac{e^{i\theta}}{q}\left(1-\frac{c}{\rho}\right)(\overline{\omega_\sigma}). \tag{41}$$

From (41) it follows that

$$z_{\bar{\sigma}} = \lambda z_{\sigma}, \tag{42}$$

where

$$\lambda = \mathscr{L} \frac{\overline{(\omega_{\sigma})}}{\omega_{\sigma}}; \qquad \mathscr{L} = \frac{1 - c/\rho}{1 + c/\rho}. \tag{43}$$

Notice that λ is complex and depends implicity on z through $\mathscr{L}$. For future reference we note te following properties of λ which are analogous to the same as μ and can be proved in a similar manner:

(1) λ is a $C^{\infty}(\Omega)$ function.

(2) $|\lambda|$ is a monotonically increasing function of the Mach number M.

(3) $|\lambda|$ is bounded between 0 and $(c-1)/(c+1)$, where c is given by (6), i.e.,

$$0 \leqslant |\lambda| \leqslant \left(\frac{c-1}{c+1}\right) < 1 \qquad \text{for} \quad 0 \leqslant M \leqslant 1. \tag{44}$$

(4) λ is $O(M^2)$ and is given by

$$\lambda = -\frac{M^2}{4} + \frac{(\gamma - 1)}{16} M^4 + O(M^6). \tag{45}$$

Notice from (46), that $\lambda = 0$ corresponds to conformal mapping. The jacobian of this mapping is given by

$$J = |z_{\sigma}|^2 - |z_{\bar{\sigma}}|^2 = (1 - \lambda^2)|z_{\sigma}|^2 > 0. \tag{46}$$

The right inequality follows from (44). Thus the mapping $z(\sigma)$ induced by the flow is well defined and can be used to generate a grid. This method of grid generation is addressed elsewhere [12].

It should be mentioned that under this mapping, image of a closed curve in Ω (σ-plane) need not be a closed curve in Ω_z (z-plane). Let the curve C in Ω_z be the image of a circle $|\sigma| = r \leqslant 1$ in the σ-plane. Let Δz denote the gap between the two end points of the curve. The gap Δz is same for any closed curve in σ-plane. From (40) we have

$$\Delta z = \frac{1}{2} \oint_{|\sigma| = r} \frac{e^{i\theta}}{q} \left\{ \left(1 + \frac{c}{\rho}\right) \omega_{\sigma} \, d\sigma + \left(1 - \frac{c}{\rho}\right) \overline{(\omega_{\sigma})} \, d\bar{\sigma} \right\}. \tag{47}$$

The variables q, ρ, θ are related to τ through (7) to (10). We have not succeeded in directly applying (47) to the closure problem in the context of inverse problems.

4. Special Cases (Incompressible and Tangent Gas Flows)

For incompressible flow,

$$M = 0; \qquad p = \text{const} = c. \tag{48}$$

Then from (4), $K = 1$ and from (14) and (43), we have

$$\mu = 0; \qquad \lambda = 0. \tag{49}$$

Equations (28) and (42) reduce to

$$\tau_{\bar{\sigma}} = 0; \qquad z_{\bar{\sigma}} = 0. \tag{50}$$

Hence τ and z are analytic functions in the σ-plane as expected.

For tangent gas flow [8–10],

$$\gamma = -1; \qquad \frac{c}{\rho} = \frac{1}{\beta}. \tag{51}$$

Then from (4), $K = 1$ and from (14) and (43), we have

$$\mu = 0; \qquad \lambda = \frac{1 - \beta^{-1}}{1 + \beta^{-1}}. \tag{52}$$

Equations (28) and (42) reduce to

$$\tau_{\bar{\sigma}} = 0; \qquad z_{\bar{\sigma}} = \frac{1 - \beta^{-1}}{1 + \beta^{-1}} z_{\sigma}. \tag{53}$$

Thus τ is an analytic function of σ. However, the mapping $z(\sigma)$ is still quasi-conformal [1, 8]. In this case the closure condition (47) admits a suitable respresentation [8].

4.1. *New Approximation*

From (20) and (29) we have

$$|\chi| = O(M^4). \tag{54}$$

It follows from Eq. (28) that $\tau_{\bar{\sigma}}$ is $O(M^4)$ and hence an $O(M^4)$ approximation of τ, denoted as τ^a, will be governed by

$$\tau^a_{\bar{\sigma}} = 0. \tag{55}$$

Since τ^a is an analytic function, it can be computed using FFT. We have addressed a similar problem in [8]. This approximate solution can be used as a starting guess

in the numerical solution of Eq. (28). It should be mentioned that this approximation (henceforth to be referred to as TA) and the tangent gas approximation (henceforth to be referred to as TGA) differ in the following two respects, even though both are $O(M^4)$ accurate [8]:

(1) In TGA, pressure-density ($p(\rho)$) relation is approximated and in GA the solution itself is approximated without any modification of $p(\rho)$ relation for an ideal gas [8, 10].

(2) In TGA, the mapping $z(\sigma)\colon \Omega \to \Omega_z$ (Eq (40)) and the closure Δz (see Eq. (47)) admit very suitable representations which makes TGA particularly attracctive for inverse airfoil design [9].

It may be worthwhile to compare the solution for the direct (analysis) problem in the TGA and GA approximations. It should be noticed that (55) forms a natural, beside being very accurate, starting guess in the numerical solution of Eq. (28).

5. Airfoil Design

This problem has been addressed by many authors. See [13–14] and references therein. In this section we describe the application of the present formulation to the airfoil design problem. The profile of an airfoil is in general smooth with either a sharp or a cusped trailing edge. Thus the data $q(s)$ over such a smooth profile can have at most two zeroes, one corresponding to the front stagnation point and the other corresponding to a sharp trailing edge. Since images of these points are $\exp(i\alpha_s)$ and 1 respectively on the unit circle, a suitable choice for the analytic function $g(\sigma)$ in Eq. (33) is

$$e^{g(\sigma)} = (1-\sigma)^{-\delta}\,(e^{i\alpha_s}-\sigma)^{-1}\exp\left(\sum_{n=0}^{\infty} c_n\sigma^n\right), \tag{56}$$

where

$$\alpha_s = \pi - 2\alpha_0 \qquad \text{and} \qquad \delta = \theta_t/\pi.$$

The first two terms in (25) account for the singularities at the stagnation points, $\sigma = 1$ and $\sigma = \exp(i\alpha_s)$. With this choice of $g(\sigma)$ we have from (33)

$$\tau - \tau^p = \ln[(1-\sigma)^{-\delta}\,(e^{i\alpha_s}-\sigma)^{-1}] + \sum_{n=0}^{\infty} c_n\sigma^n \tag{57}$$

which we rewrite as

$$\tilde{\tau} - \tau^p(\sigma) = \sum_{n=0}^{\infty} c_n\sigma^n. \tag{58}$$

Here and below $\tilde{\tau}$ refers to

$$\tilde{\tau} = \tau - \ln[(1-\sigma)^{-\delta}(e^{i\alpha_s}-\sigma)^{-1}] \tag{59}$$

which assumes finite values at the stagnation points. Thus the Eq. (57) has been regularized in the form (58) which is suitable for numerical purpose. In analogy with (10), we write

$$\tilde{\tau} = \tilde{v} + i\tilde{\theta}. \tag{60}$$

Projection of Eq. (58) and (59) on the unit circle gives

$$\tilde{\tau}(\alpha) - \tau^p(\alpha) = \sum_{n=0}^{N/2-1} c_n e^{in\alpha}. \tag{61}$$

and

$$\tilde{\tau}(\alpha) = \tau(\alpha) - \ln[(1-e^{i\alpha})^{-\delta}(e^{i\alpha_s}-e^{i\alpha})^{-1}]. \tag{62}$$

Notice that the series has been truncated to a finite sum for numerical purposes. From (60) and (62), we have

$$\tilde{v}(\alpha) = -v(\alpha) - \ln G(\alpha) \tag{63}$$

and

$$\tilde{\theta}(\alpha) = \theta(\alpha) - \eta(\alpha), \tag{64}$$

where $G(\alpha)$ and $\eta(\alpha)$ are given by

$$G(\alpha) = \left(2\sin\frac{\alpha}{2}\right)^{-\delta}\left|2\cos\left(\alpha_0+\frac{\alpha}{2}\right)\right|^{-1} \tag{65}$$

and

$$\eta(\alpha) = \frac{1}{2}\delta(\pi-\alpha) - \left(\pi+\frac{\alpha}{2}\right) + \pi U(\alpha-\alpha_s) + \alpha_0. \tag{66}$$

Equation (64) can be written in terms of the body angle as

$$\tilde{\theta}(\alpha) = \theta_B(\alpha) - \frac{1}{2}\delta(\pi-\alpha) + \frac{\alpha}{2} - (\pi+\alpha_0). \tag{67}$$

6. Numerical Method

6.1. *Computational Steps (Flow Chart)*

As mentioned earlier, our method is based on the algorithm discussed in Section 3.2. Computations are performed within the unit circle with M grids in the radial direction and N grids in the angular direction. In our algorithm the

free stream Mach number M_∞ is free to be determined by the following algorithm. Our algorithm involves the following steps:

(a) Compute $q(\alpha_k)$ and hence $v(\alpha_k)$ at $\alpha_k = (2\pi/N)\,k$; $k \in [0, N-1]$, from the given data $q(s)$ using (22) and (27). For details see [2].

(b) Compute $\tilde{v}(\alpha_k)$ from (63) and (65) at $\alpha_k = (2\pi/N)\,k$; $k \in [0, N-1]$.

(c) Assume $\tau_{jk}^p = 0$; $i \in [0, M-1]$; $k \in [0, N-1]$. This is the initial guess.

(d) Find the complex conjugate $\tilde{\theta}(\alpha_k) - \mathrm{Imag}(\tau_{jk}^p(\alpha_k))$ from $\tilde{v}(\alpha_k) - \mathrm{Real}(\tau_{jk}^p(\alpha_k))$ using (61). Back-to-back fast Fourier transform is used for this purpose. The values of the body angle $\theta_B(\alpha_k)$ are computed from $\tilde{\theta}(\alpha_k)$ using (67). The shape of the profile is then obtained from (32).

(e) Find $g_{jk} = g(\sigma_{jk})$; $j \in [0, M-1]$, $k \in [0, N-1]$ using the Taylor series (58). Again FFT is used to sum the Taylor series which favors considerable computational savings.

(f) Find τ_{jk}^p; $j \in [0, M-1]$, $k \in [0, N-1]$. Even though computation of the double integral in (C.9) (See Appendix C.) at $M \times N$ points might be intimidating computationally, such is not the case when care is taken to optimize the code on a vector computer with an appropriate number of memory banks.

The updated value of τ_{jk}^p in step (f) becomes the input to the step (d) above. The steps (d) to (f) are carried out in an iterative loop until some convergence criterion is met. A suitable quantity to monitor for convergence is $\Delta\theta = \max_{0 \le k \le N} |\tilde{\theta}_{B,k}^{j+1} - \tilde{\theta}_{B,k}^{j}|$, j denoting the level of iteration. When $\Delta\theta_B$ is below some tolerance level, the iteration scheme may be considered to have converged. The shape of the boundary, obtained in step (d) at convergence, is the solution to the inverse problem. At convergence the free stream Mach number is obtained from the real part v of $\tau(\sigma = 0)$ (see Eq. (9)). In all our cases discussed in the next section, the number of iterations did not exceed four with the tolerance $= 10^{-5}$.

In our algorithm the free stream Mach number M_∞ is a free parameter and is obtained from $v(\sigma = 0)$ (see Eq. (9)). $v(\sigma = 0)$ is the real part of $\tau(\sigma = 0)$ which is obtained from our converged solution. Since our solution at zeroth order is $O(M^4)$, the computed M_∞ at zeroth order is very close to the converged value. In fact in all our runs the M_∞ during iterations were same up to two decimal places. Therefore for subcritical flows, the computed free stream Mach number M_∞ could not get close to 1. Infact this method will work for all possible subcritical input data (speed).

6.2. *Evaluation of the Double Integral (Eq. (34))*

The evaluation of τ_p given by (see Appendix C),

$$\tau^p = -\frac{1}{\pi}\iint_\Omega \frac{f(\zeta)}{\zeta - \sigma}\, d\xi\, d\eta$$

$$= \frac{f(\sigma)}{\sigma} - \frac{1}{\pi}\iint_\Omega \frac{f(\zeta) - f(\sigma)}{\zeta - \sigma}\, d\xi\, d\eta$$

involves numerical computation of the above double integral. Numerically the second form is more suitable for obvious reasons. The computation of this double integral is done by using an elementary composite trapezoidal rule. Each iteration involves evaluation of this integral at $M \times N$ grid points in $\Omega: |r| \leqslant 1$ and each evaluation takes an $O(M \times N)$ operation count. Therefore the total number of operation counts devoted to this integral evaluation is $O(M^2N^2)$ per iteration, which accounts for the major fraction of the computation time on a scalar machine. However, in practice this computation does not require much time and results are obtained in a fraction of a second in CPU time with 65×32 grids, which is typical for our problem. Our code has been completely vectorized on CRAY X-MP at the San Diego supercomputer center. We have run our code on CRAY X-MP resulting in substantial speedup over running the code on the local MIPs machine which is itself a fast machine (peak speed nearly 7 Mflops).

As mentioned earlier an effective strategy to accelerate the computation further is possible by devising an efficient method for the evaluation of the double integral. Such an approach would involve writing the integral as a power series in σ and would be similar in spirit to [3, 4]. However such an effort has not yet been pursued.

7. Preliminary Results (Validation)

To explore the validity of our method, we focus here on three aspects: (1) numerical convergence; (2) rate of convergence; and (3) quantitative comparison of the computed solution with the exact solution.

In our method, the boundary data is the prescribed speed distribution. We generate such data over known airfoils by using the Euler code FLO52s (analysis mode) [11]. Specifically we chose a 12% thick Kutta airfoil and a NACA0012 airfoil. The philosophy here is to generate the profiles using these data as input (inverse mode) and compare these profiles with the exact known airfoils. Even though the analysis and the inverse modes are theoretically exact inverses of each other, numerically there is minor deviation due to the differences in the numerics of the Euler code (analysis mode), which provides the input data, and that of our code (inverse mode), which provides the airfoil.

Figure 2 shows the speed distribution over the Kutta airfoil at $M_\infty = 0.6$ and $\alpha = 0.0$. With this data as input, our code is run. We used 129 points in the circular direction and 31 points in the radial direction. We obtain a converged solution and a free stream Mach number M_∞^c within three iterations. Convergence criterion in this and all the following cases is taken to be the maximum of the difference in the values of the body angle between two successive iterations below some tolerance level. Figure 3 and Fig. 4 respectively compare the zeroth-order solution and the converged solution (produced by our code) with the exact solution. As seen in Fig. 3 the zeroth-order solution generated by our code compares well with the exact solution. This is to be expected since the nonlinear contribution is very mild (see

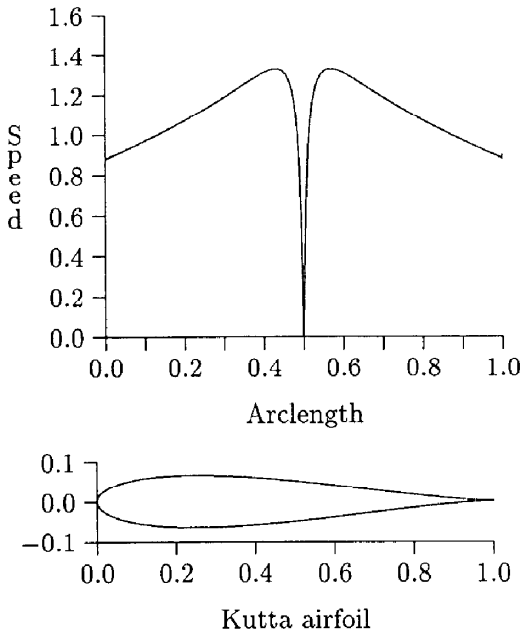

FIG. 2. Normalized speed distribution over a 12% thick Kutta airfoil at Mach number $M = 0.6$ and $\alpha = 0.0$.

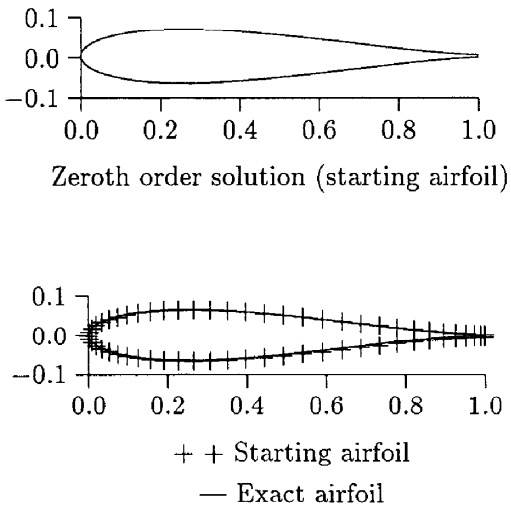

FIG. 3. Comparison of the zeroth order solution (initial guess of the airfoil generated by our code) and the exact solution (Kutta airfoil).

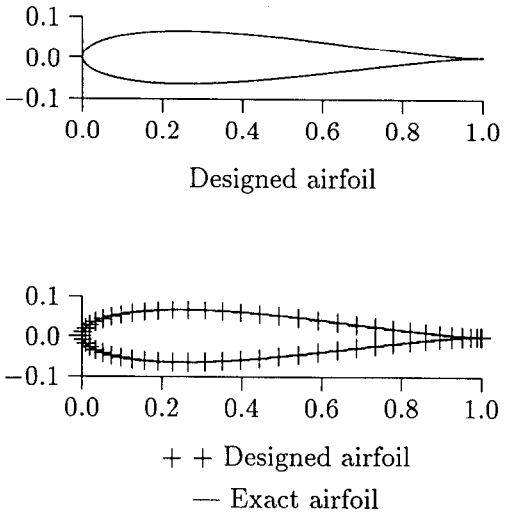

FIG. 4. Comparison of the converged solution and the exact solution (Kutta airfoil).

Section 3.3). The computed free stream Mach number $M_\infty^c = 0.5999$ is very close to the exact value $M_\infty = 0.6$. This much error is probably well within the acceptable range. Figure 5 shows the convergence rate. Here we plot the error (maximum of the difference in the values of the body angle between two successive iterations) as a function of number of iterations. We see that the convergence is indeed very rapid.

It should be mentioned that even though the airfoil that we have generated seems to agree visually with the exact airfoil, there is a small amount of gap (about 0.05% of the chord thickness) at the trailing edge. Because of this gap we have not tried

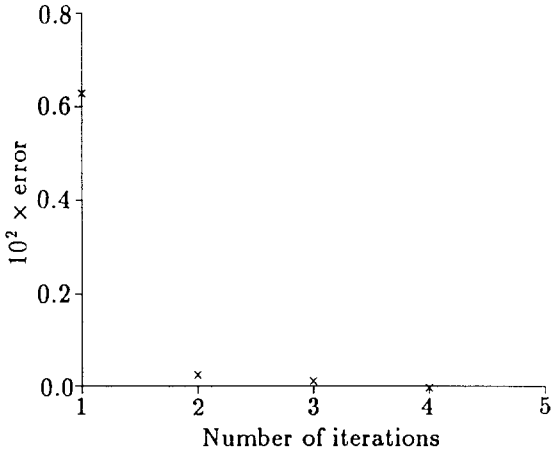

FIG. 5. Convergence rate of the solution.

to compute the solution over the designed airfoil in order to compare this with the input speed distribution. Since we generate our profile here by integrating the solution (see Eq. (32)), any small error in the computed value of the body angle will generate a finite gap, even though ideally it should be zero. Our numerical solution is very accurate except at two points around the leading edge where the pointwise error in the body angle is about 1.0%. This error is the source of the minor gap at the trailing edge.

In the following we show some results with the NACA0012 airfoil. This airfoil has a sharp trailing edge and thus the speed at the trailing edge is zero. In Fig. 6 we plot the Euler speed distribution as a function of arclength of this airfoil at $M = 0.6$ and $\alpha = 0.0$. With this as input our code generates the body angle. Here again our solution turns out to be virtually exact except at two points near the leading edge where the error in the body angle is within 2%. Here we generate the airfoil by integrating Eq. (32) on either side of the airfoil up to the front stagnation points with minor smoothing of the data at the leading edge. Figure 7 compares the zeroth-order solution with the exact airfoil. Here the solution turns out to be excellent and convergence is achieved in three iterations. The converged solution is shown in Fig. 8. The computed value of the free stream Mach number is $M_\infty^c = 0.6013$ which is close to the exact value 0.6. This solution is obtained with 129 points in the circular direction and 31 points in the radial direction. The CPU time for each of the runs were about one minute on the MIPs machine.

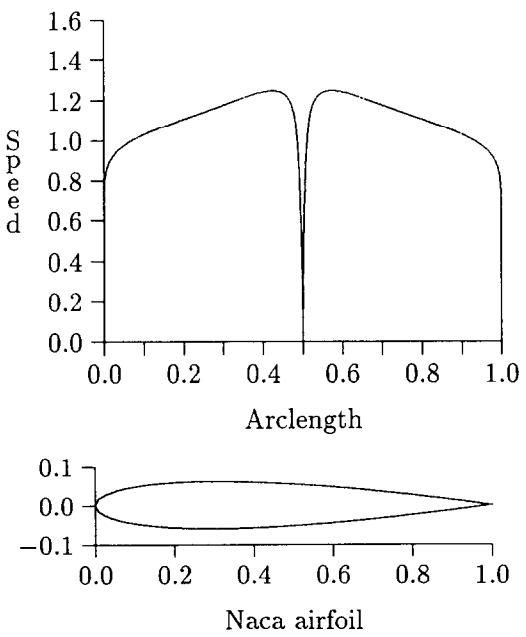

FIG. 6. Normalized speed distribution over a 12% thick NACA0012 airfoil at Mach number $M = 0.6$ and $\alpha = 0.0$.

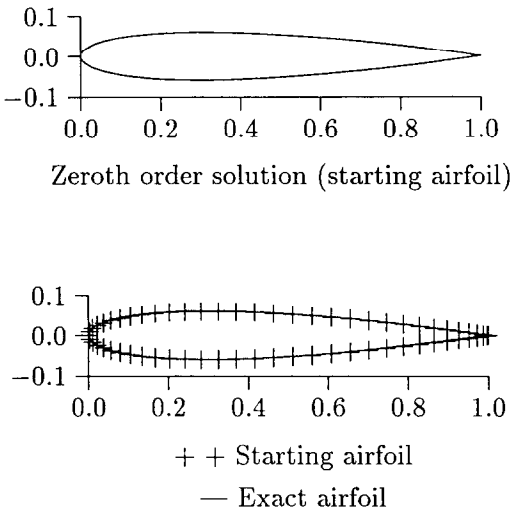

FIG. 7. Comparison of the zeroth-order solution (initial guess of the airfoil generated by our code) and the exact solution (NACA0012 airfoil).

8. CONCLUSION

Here we have developed the Beltrami formulation for compressible flow equations. We have discussed some of its properties in regard to the flow. This formulation is applicable to subcritical flows in general and various problems for subcritical

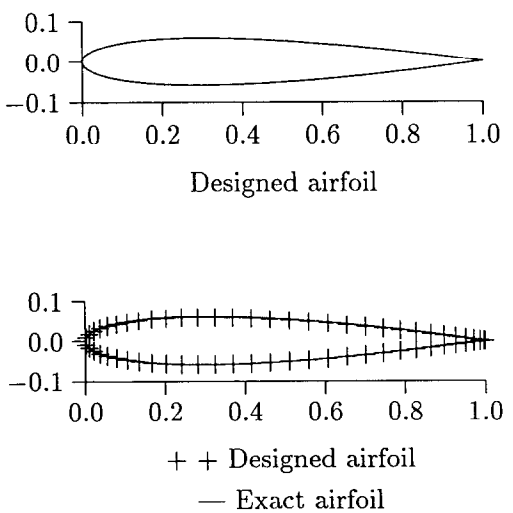

FIG. 8. Comparison of the converged solution and the exact solution (NACA0012 airfoil).

flows can also be solved by using the present formulation. An algorithm for solving this equation is provided which has been shown to be convergent on a model problem (the inverse problem). This algorithm provides an alternative to solve the Beltrami equation. Since any quasi-linear PDE can be cast into this form [2], the algorithm provided here has general applicability. However, there is considerable room for improvement in speeding up the computation using this algorithm. The present method of computation of the double integral (see Section 6.2) is the only minor bottleneck which can be improved as mentioned earlier.

We have applied this formulation to the inverse airfoil design problem. Our algorithm for this problem is valid for arbitrary subcritical input data as discussed in Section 6.1. Since the zeroth order solution is $O(M^4)$ accurate, the convergence rate speeds up with decreasing M_∞. In fact for low speed, the zeroth-order solution will suffice for all practical purposes. We have generated airfoils with symmetric speed distributions as input data. However, the present version of the vectorized code needs further coding for the nonsymmetric case. The main difficulty in regard to the inverse problem is the closure problem which has not yet been addressed using our formulation. It should be mentioned that previously we have also provided a convergent algorithm for solving the PDEs (see Eq. (3)) in the real plane by using a finite difference scheme [2].

The present method of inverse airfoil design has several advantages over other methods: (1) The $O(M^4)$ accurate solution is obtained by only one FFT. This also gives the free stream Mach number which is almost exact for reasons mentioned earlier; (2) the numerical convergence is very rapid and in many instances zeroth-order solution will suffice; (3) the stagnation point singularities are better resolved due to inherent smoothing properties of the integral (see Eq. 34); (4) the formulation developed here is very general and is applicable to other compressible flow problems. The only limitation of this method is that it is applicable to subcritical flows.

APPENDIX A: Solution to the Beltrami equation $u_{\bar{z}} = f$

If

$$u_{\bar{z}} = f \tag{A1}$$

and f satisfies a Hölder condition with exponent α in a circle Ω: $|z| < r$, then

$$u(z) = -\frac{1}{\pi} \iint_\Omega \frac{f(\zeta)}{\zeta - z}\, d\xi\, d\eta, \tag{A2}$$

$$u_{\bar{z}} = -\frac{1}{\pi} \iint_\Omega \frac{f(\zeta) - f(z)}{(\zeta - z)^2}\, d\xi\, d\eta, \tag{A3}$$

where $\zeta = \xi + i\eta$.

We have roughly quoted the above from [2] and here we prove it for the sake of completeness.

Proof. Let

$$u = 4v_z \qquad \text{in} \quad \Omega. \tag{A4}$$

Then from (A1) we have

$$4v_{z\bar{z}} = f(z). \tag{A5}$$

Therefore,

$$v = -\frac{1}{2\pi}\iint_{\Omega} f(\xi, \eta)\log|\zeta - z|\, d\xi\, d\eta$$

and hence

$$\begin{aligned} v_z &= \frac{1}{2\pi}\iint_{\Omega} f(\xi, \eta)\frac{d}{dz}\{\log|\zeta - z|\}\, d\xi\, d\eta \\ &= \frac{1}{4\pi}\iint_{\Omega} f(\xi, n)\frac{d}{dz}\{\log(\zeta - z) + \log\overline{(\zeta - z)}\}\, d\xi\, d\eta \\ &= \frac{1}{4\pi}\iint_{\Omega}\frac{f(\xi, \eta)}{\zeta - z}\, d\xi\, d\eta + \frac{1}{4\pi}\iint_{\Omega} f(\xi, \eta)\frac{d}{dz}\{\log\overline{(\zeta - z)}\}\, d\xi\, d\eta. \end{aligned} \tag{A6}$$

In the second integral, $\log\overline{(\zeta - z)}$ is singular at $\zeta = z$. If we exclude a small ball B of radius R with center at z, and boundary ∂B, then $\log\overline{(\zeta - z)}$ is analytic in $\Omega - B$. Therefore, for the second integral, we have

$$\begin{aligned} &\frac{1}{4\pi}\iint_{\Omega} f(\xi, \eta)\frac{d}{dz}\{\log\overline{(\zeta - z)}\}\, d\xi\, d\eta \\ &= \frac{-1}{4\pi}\iint_{B} f(\xi, v)\frac{d}{d\zeta}\log\overline{(\zeta - z)}\, d\xi\, d\eta \\ &= -\frac{1}{4\pi}\iint_{B}\frac{d}{d\zeta}(f(\xi, \eta)\log\overline{(\zeta - z)})\, d\xi\, d\eta + \frac{1}{4\pi}\iint_{B}\frac{df}{d\zeta}\log\overline{(\zeta - z)}\, d\xi\, d\eta \\ &= -\frac{i}{8\pi}\int_{\partial B} f(\xi, \eta)\log\overline{(\zeta - z)}\, d\bar{\zeta} + \frac{1}{4\pi}\iint_{B}\frac{df}{d\zeta}\log\overline{(\zeta - z)}\, d\xi\, d\eta \\ &= +\frac{1}{8\pi}\int_{0}^{2\pi} f(\xi, \eta)\log\overline{(\zeta - z)}\, R\, d\theta + \frac{1}{4\pi}\int_{0}^{2\pi}\int_{0}^{R}\frac{df}{d\zeta}\log\overline{(\zeta - z)}\, r\, dr\, d\theta \end{aligned} \tag{A7}$$

Since both of the integrands are continuous and tend to zero as $R \to 0$, the above integral is zero and we have from (A6),

$$v_z = \frac{1}{4\pi} \iint_\Omega \frac{f(\xi, \eta)}{\zeta - z} d\xi \, d\eta$$

and

$$v_{zz} = \frac{-1}{4\pi} \iint_\Omega \frac{f(\xi, \eta)}{(\zeta - z)^2} d\xi \, d\eta. \tag{A8}$$

Since

$$\begin{aligned} \iint_\Omega \frac{d\xi \, d\eta}{(\zeta - z)^2} &= -\iint_\Omega \frac{d}{d\zeta}\left(\frac{1}{\zeta - z}\right) d\xi \, d\eta \\ &= -\frac{i}{2} \oint \frac{d\bar{\zeta}}{\zeta - z} \\ &= \frac{ir^2}{2} \oint \frac{d\zeta}{\zeta^2(\zeta - z)} \\ &= 0, \end{aligned} \tag{A9}$$

we have, from (A8) and (A9),

$$v_{zz} = \frac{-1}{4\pi} \iint_\Omega \frac{f(\zeta) - f(z)}{(\zeta - z)^2} d\xi \, d\eta. \tag{A10}$$

From (A6) and (A4) we get

$$u = -\frac{1}{\pi} \iint_\Omega \frac{f(\xi, \eta)}{\zeta - z} d\xi \, d\eta \tag{A2}$$

and from (A6) and (A10) we have

$$\begin{aligned} u_z &= 4v_{zz} \\ &= -\frac{1}{\pi} \iint_\Omega \frac{f(\zeta) - f(z)}{(\zeta - z)^2} d\xi \, d\eta. \end{aligned} \tag{A3}$$

APPENDIX B

We want to evaluate the mean value of (A2) on the boundary ∂B of a unit circle, i.e.,

$$\int_0^{2\pi} u(\alpha) \, d\alpha = \int_0^{2\pi} \left(\iint_\Omega \frac{f(\zeta)}{\zeta - e^{i\alpha}} d\xi \, d\eta \right) d\alpha.$$

If we denote the above integral by I, then we have

$$I = \iint_{\Omega} f(\zeta)\, P_0(\zeta)\, d\xi\, d\eta, \tag{B1}$$

where

$$P_0(\zeta) = \int_0^{2\pi} \frac{d\alpha}{\zeta - e^{i\alpha}}. \tag{B2}$$

Using the notation $\theta = e^{i\alpha}$, we have from (B2)

$$\begin{aligned} P_0(\zeta) &= -i \oint \frac{d\theta}{\theta(\zeta - \theta)} \\ &= -\frac{i}{\zeta}\left\{\oint \frac{d\theta}{\theta} + \oint \frac{d\theta}{\zeta - \theta}\right\} \\ &= -\frac{i}{\zeta}\left[2\pi i + \begin{cases} -2\pi i & \text{if } \zeta \notin \partial B \\ -\pi i & \text{if } \zeta \in \partial B \end{cases}\right] \\ &= \begin{cases} 0 & \text{if } \zeta \notin \partial B. \\ \pi/\zeta & \text{if } \zeta \in \partial B. \end{cases} \end{aligned} \tag{B3}$$

From (B1) and (B3) we have

$$I = 0. \tag{B4}$$

APPENDIX C: Evaluation of τ^p

The nonanalytic part τ_p of the solution is of the form (see Eq. (34)):

$$\tau_p = -\frac{1}{\pi} \iint_{\Omega} \frac{f(\zeta)}{\zeta - \sigma}\, d\xi\, d\eta. \tag{C.1}$$

This singular integral is desingularized for numerical purposes in the following manner: We first write τ_p as:

$$\begin{aligned} \tau^p &= -\frac{1}{\pi} \iint_{\Omega} \frac{f(\zeta)}{\zeta - \sigma}\, d\xi\, d\eta \\ &= -\frac{1}{\pi} \iint_{\Omega} \frac{f(\zeta) - f(\sigma)}{\zeta - \sigma}\, d\xi\, d\eta - \frac{f(\sigma)}{\pi} \iint_{\Omega} \frac{d\xi\, d\eta}{\zeta - \sigma}. \end{aligned} \tag{C.2}$$

The second integral in (C.2) can be explicitly evaluated as follows: We write this integral as

$$\iint_{\Omega} \frac{d\xi\, d\eta}{\zeta - \sigma} = \iint_{\Omega} \frac{d}{d\zeta} (\ln(\zeta - \sigma))\, d\xi\, d\eta. \tag{C.3}$$

Excluding a small ball B of radius ε with center at σ and applying Green's formulae, we have

$$\iint_{\Omega - B} \frac{d\xi\, d\eta}{\zeta - \sigma} = \frac{i}{2}\left[\oint_{\partial\Omega} \ln(\zeta - \sigma)\, d\bar{\zeta} - \oint_{\partial B} \ln(\zeta - \sigma)\, d\bar{\zeta}\right]. \tag{C.4}$$

The region $(\Omega - B)$ is bounded by $\partial\Omega$ and ∂B. Since

$$\zeta\bar{\zeta} = \begin{cases} 1; & \text{on } \partial\Omega \\ \varepsilon^2; & \text{on } \partial B, \end{cases}$$

we have from (C.4)

$$\begin{aligned} \int_{\Omega - B} \frac{d\xi\, d\eta}{\zeta - \sigma} &= -\frac{i}{2}\left[\oint_{|\zeta| = 1} \frac{\ln(\zeta - \sigma)}{\zeta^2}\, d\zeta - \varepsilon^2 \oint_{|\zeta - \sigma| = \varepsilon} \frac{\ln(\zeta - \sigma)}{\zeta^2}\, d\zeta\right] \\ &= -\frac{i}{2}\left[\oint_{|\zeta| = \varepsilon} \frac{\ln(\zeta - \sigma)}{\zeta^2}\, d\zeta + (1 - \varepsilon^2) \oint_{|\zeta - \sigma| = \varepsilon} \frac{\ln(\zeta - \sigma)}{\zeta^2}\, d\zeta\right]. \end{aligned} \tag{C.5}$$

Application of residue theorem gives

$$\oint_{|\zeta| = \varepsilon} \frac{\ln(\zeta - \sigma)}{\zeta^2}\, d\zeta = 2\pi i \left[\frac{d}{d\zeta} \ln(\zeta - \sigma))\right]_{\zeta = 0} = -\frac{2\pi i}{\sigma}. \tag{C.6}$$

It is not difficult to see that the integral around the logarithmic singularity will go to zero as the singularity is approached, i.e.,

$$\lim_{\varepsilon \to 0} \oint_{|\zeta - \sigma| = \varepsilon} \frac{\ln(\zeta - \sigma)}{\zeta^2}\, d\zeta = 0. \tag{C.7}$$

Substituting (C.6) and (C.7) in (C.5) and taking the limit $\varepsilon \to 0$, we have,

$$\iint_{\Omega} \frac{d\xi\, d\eta}{\zeta - \sigma} = -\frac{\pi}{\sigma} \tag{C.8}$$

From (C.2) and (C.8) we have

$$\tau^p = \frac{f(\sigma)}{\sigma} - \frac{1}{\pi} \iint_{\Omega} \frac{f(\zeta) - f(\sigma)}{\zeta - \sigma}\, d\xi\, d\eta. \tag{C.9}$$

This desingularized version of the integral is suitable for numerical computation. Notice that the integrand in (C.9) as $\zeta \to \sigma$ has to be understood in the following sense.

Simple algebraic calculation shows that

$$\lim_{\zeta \to \sigma} \frac{f(\zeta) - f(\sigma)}{\zeta - \sigma} = \frac{\partial f}{\partial \sigma} + \frac{\partial f}{\partial \bar{\sigma}} \cos 2\alpha, \tag{C.10}$$

where α is the direction in which ζ approaches σ. Notice that for analytic $f(\zeta)$, the limit in (C.10) is defined in the usual sense.

ACKNOWLEDGMENTS

It is a pleasure to thank Tom Vogel for careful editing of the manuscript. This research, in part, has been supported by NSF Grant DMS-8803669 to Texas A & M University. The allocation of the computer resources by the San Diego supercomputer resources is gratefully acknowledged.

REFERENCES

1. L. BERS, *Mathematical Aspects o Subsonic and Transonic Gas Dynamics* (Wiley, New York, 1958), p. 164.
2. P. DARIPA, *Q. Appl. Math.* **46**, No. 3, 505 (1988).
3. V. ROKHLIN, *J. Comput. Phys.* **60**, 187 (1985).
4. L. GREENGARD AND V. ROKHLIN, *J. Comput. Phys.* **73**, 325 (1987).
5. H. W. LIEPMANN AND A. ROSHKO, *Elements of Gas Dynamics* (Wiley Interscience, New York, 1957), p. 439.
6. R. COURANT AND D. HILBERT, *Methods of Mathematical Physics, Vol. II* (Wiley Interscience, New York, 1961), p. 830.
7. P. HENRICI, *Applied and Computational Complex Analysis*, Vol. 3 (Wiley, New York, 1986).
8. P. DARIPA, AND L. SIROVICH, *J. Comput. Phys.* **62**, 400 (1986).
9. P. DARIPA, AND L. SIROVICH, *J. Comput. Phys.* **63**, 311 (1986).
10. L. C. WOODS, *The Theory of Subsonic Plane Flow* (Cambridge Univ. Press, London/New York, 1961).
11. A. JAMESON, *Transonic Shock and Multidimensional Flows*, edited by R. E. Meyer (Academic Press, New York/London, 1982), p. 37.
12. P. DARIPA, to appear.
13. F. BAUER, P. R. GARABEDIAN, AND D. KORN, *Supercritical Wing Sections III* (Springer-Verlag, New York/Berlin, 1977), p. 296.
14. H. SOBIECZKY AND A. R. SEEBASS, *Ann. Rev. Fluid Mech.* **16**, 337 (1984).